Introduction to Turbulence

Rahul Pandit

Centre for Condensed Matter Theory

Department of Physics, Indian Institute of Science, Bangalore

16 February 2009, SN Bose Centre, Kolkata

Group

Outline

- Motivation
- Models
- Results: Overview
- Phenomenology
- Direct Numerical Simulations

Motivation

- Experiments
- Numerical Studies
- Early theory and phenomenology

Turbulence: the arts

Figure 1: Miniature painting: Raga Malhar.

Turbulence: the arts

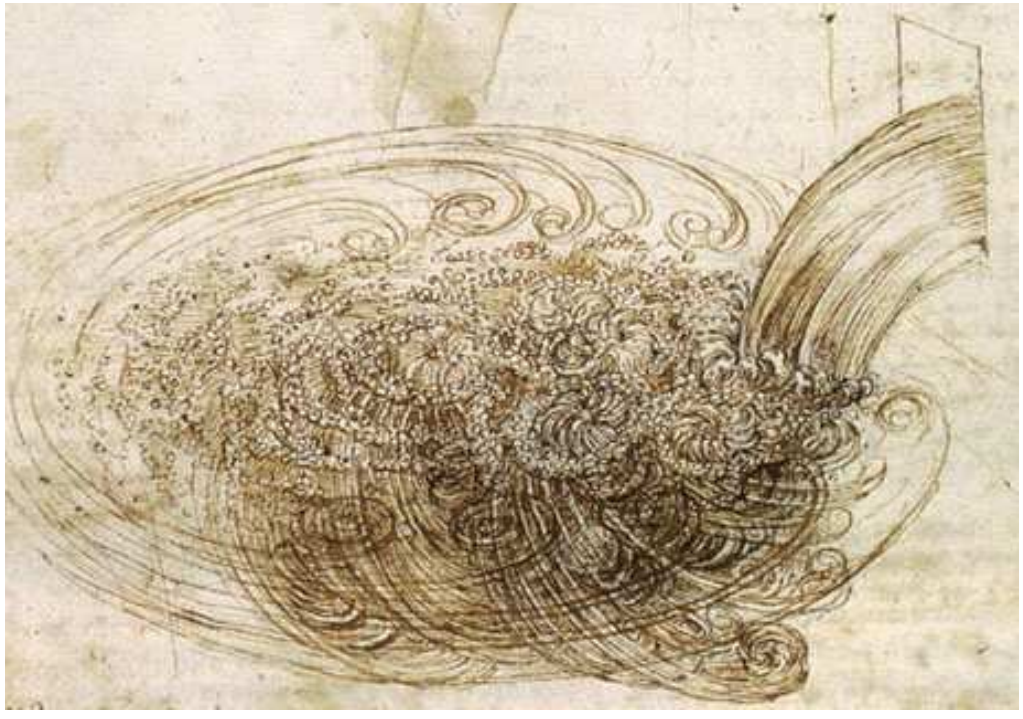

Figure 2: Eddies: Da Vinci.

Turbulence: the arts

Figure 3: Giant wave: Hokusai.

Experiments (fluids, plasmas, tracers)

- Flow visualisation
- Energy dissipation
- Correlation and structure functions
- Probability distributions

Fluid Turbulence

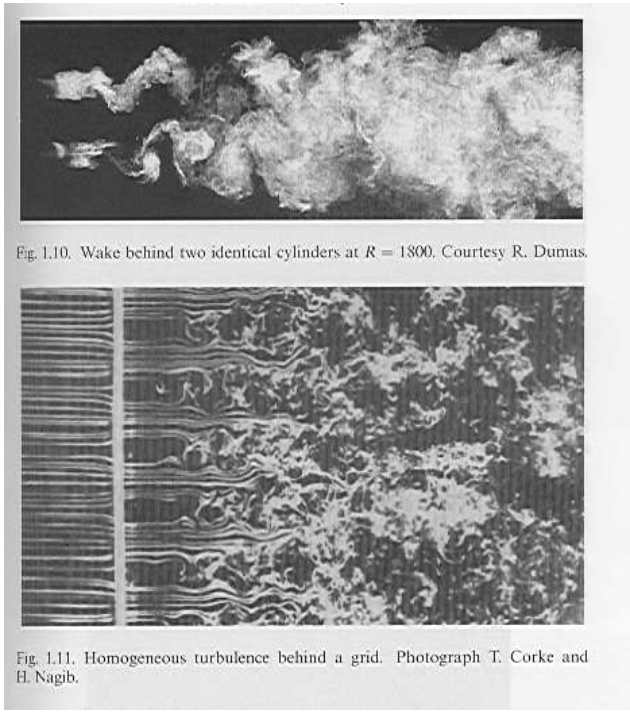

Fig. 1.10. Wake behind two identical cylinders at $R = 1800$. Courtesy R. Dumas.

Fig. 1.11. Homogeneous turbulence behind a grid. Photograph T. Corke and H. Nagib.

Figure 4: Wake behind two cylinders (top) and homogeneous turbulence behind a grid (bottom).

Fluid Turbulence

Decaying, homogeneous and isotropic fluid turbulence, behind a grid

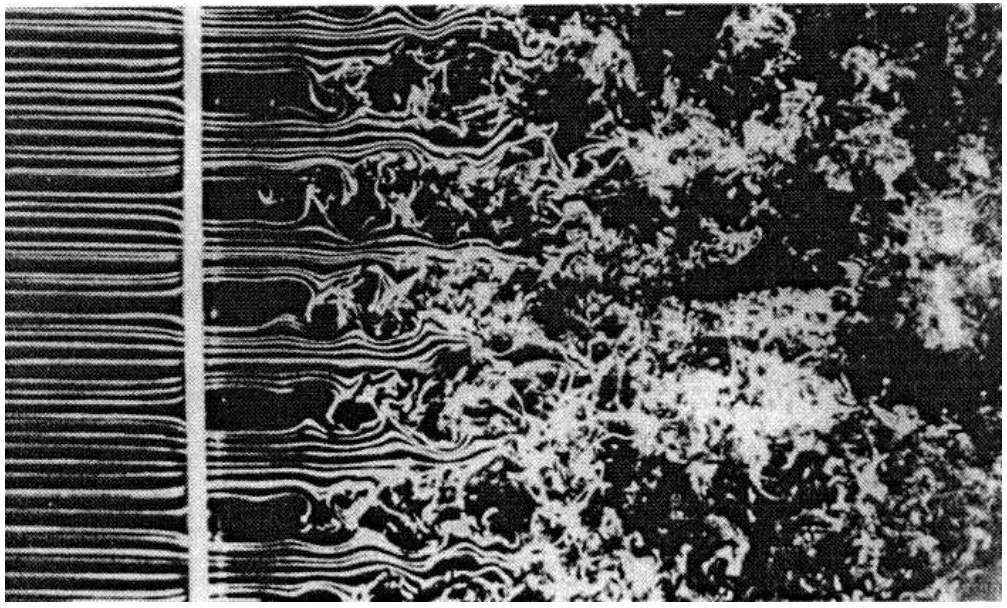

Use hot-wire anemometry to measure the velocity

Reynolds number $Re \equiv \ell U/\nu$

Osborne Reynolds

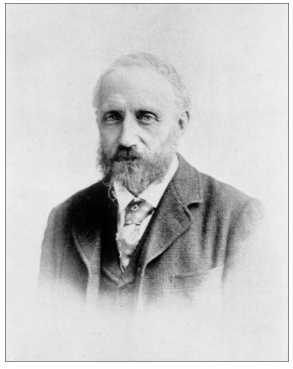

Figure 5: Copyright Universty of Manchester

Jets

- Turbulent jet of water without and with 50ppm polyethylene oxide at $Re \sim 225$
  [Hoyt (1977)]

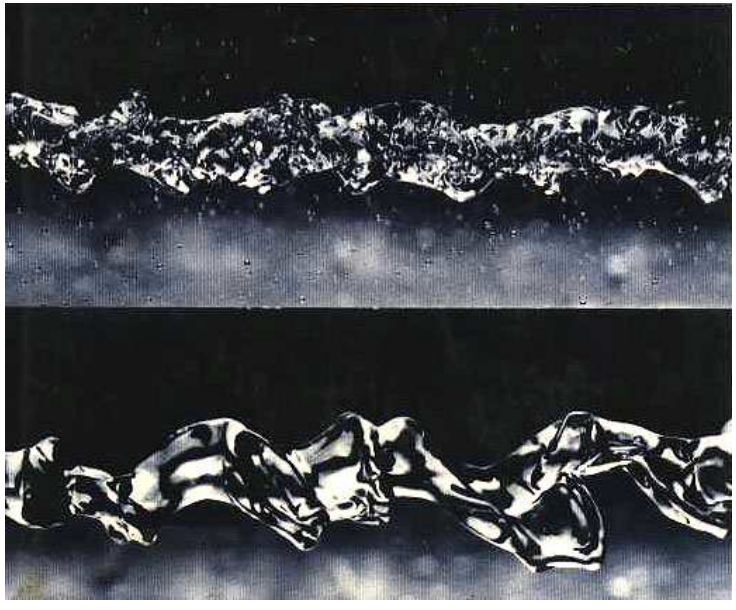

Passive Scalars

Turbulent dispersion of small particles

Mount St. Helens on May 18, 1980.
http://milou.msc.cornell.edu/lay_turb.html

Vortex filaments

FIG. 1.

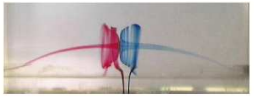

FIG. 3.

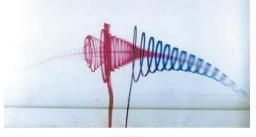

FIG. 2(a).

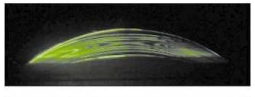

FIG. 4.

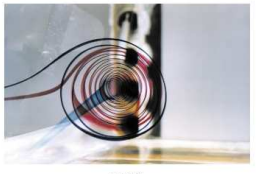

FIG. 2(b).

Visualizations of Vortex Filaments

Submitted by
F. Bottausci and P. Petitjeans, Laboratoire de Physique et Mécanique des Milieux Hétérogènes, ESPCI, Paris, France

Visualizations of stretched vortices are presented which model concentrated vorticity filaments in turbulent flows. These are known to play an important role in the intermittency. Because of the difficulties associated with working on filaments in real turbulence, we isolate such a structure from its turbulent background. A vortex filament is created by stretching (through suction) the vorticity of a laminar boundary layer flow. This coherent structure is visualized (see pictures) and characterized as a function of the initial vorticity and of the stretching.

Visualizations are obtained by injecting dye jets from upstream (Figs. 1–3) or by the laser induced fluorescence technique (Fig. 4). Depending on the parameters (flow rate of the suction and main flow rate of the channel), the vortex either persists or breaks up. In the latter case, the vortex is generated, then begins to oscillate and breaks up into a turbulent spot. Even in the former case, the vortex can be unstable, and it produces pairs of counterrotating rolls around and along itself (Fig. 4). These rolls appear around the main vortex with a periodicity that depends linearly on the stretching. The instability is centrifugal in nature. The Rayleigh criterion on the azimuthal velocity $v_\theta(r)$ can be negative outside the core of the vortex.

1070-6631/2002/14(9)/S13/1/$19.00

Some lessons

- Large spatial scales: contain most of the energy.
- Small scales: Inertial and dissipation ranges.
- Small scales: Homogeneous and isotropic, to a good approximation (far from boundaries, etc.)
- Inertial-range correlation (or structure functions) are universal (reminiscent of critical phenomena).

Solar turbulence

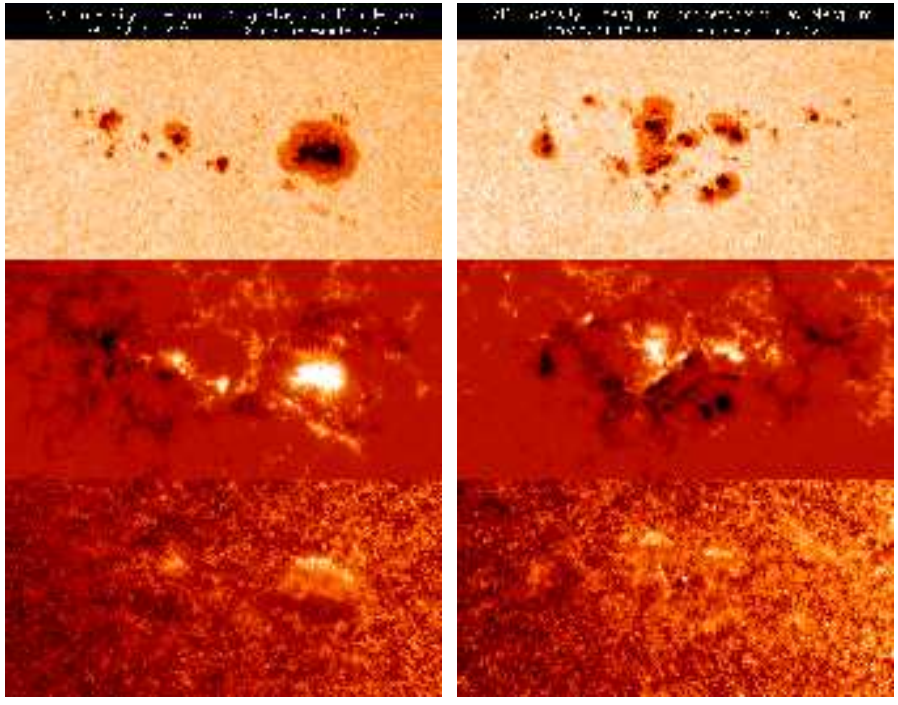

Figure 6: Turbulence on the sun: From top to bottom, optical intensity, magnetic field and velocity as measured by the SOHO project (http://soi.stanford.edu)

Boundary layers

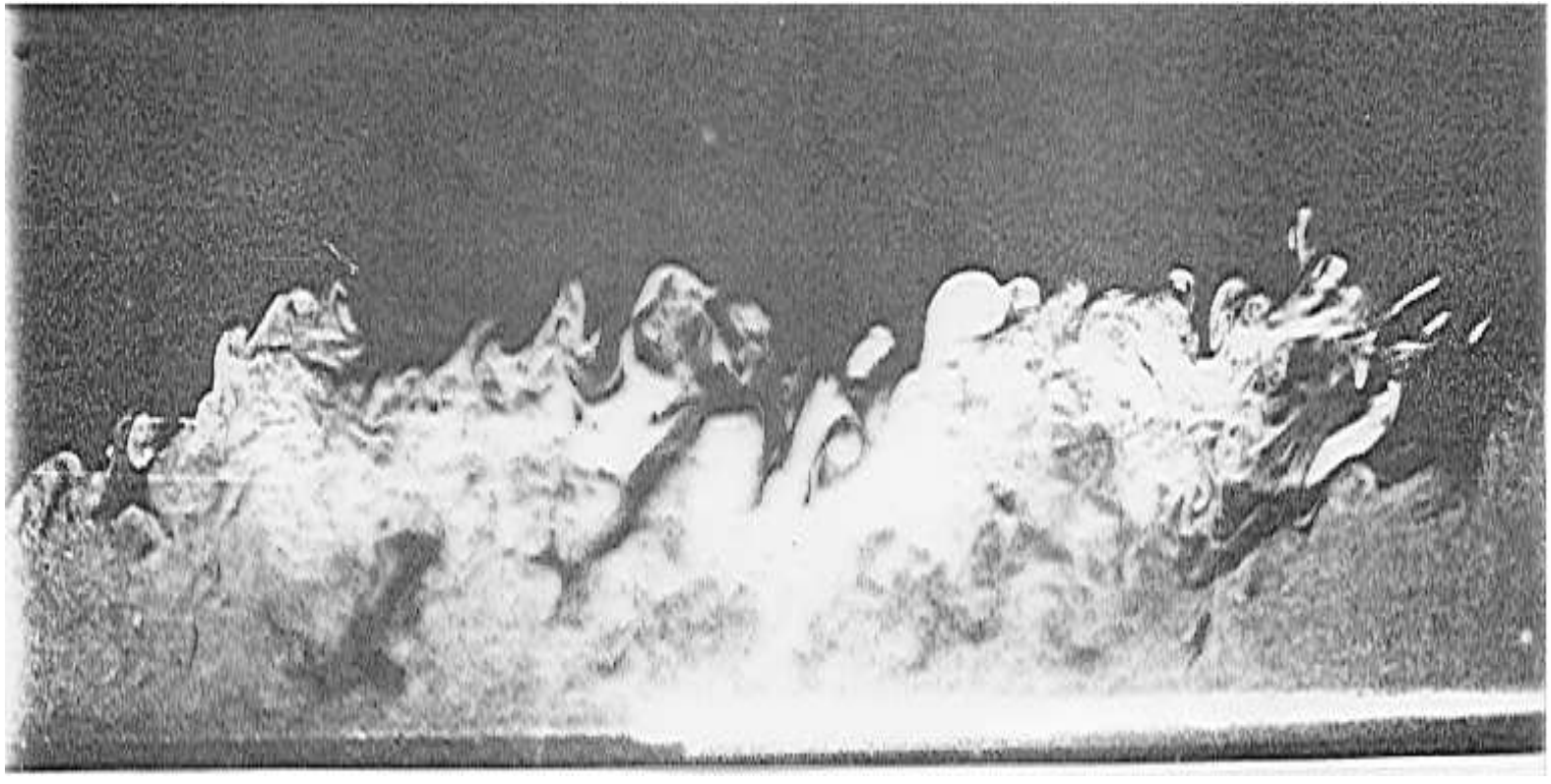

Figure 7: Turbulent boundary layer near a wall ($Re \simeq 4000$), Falco 1977.

Convection

Figure 8: Plumes in turbulent convection (Sparrow, et al., 1970)

Jets

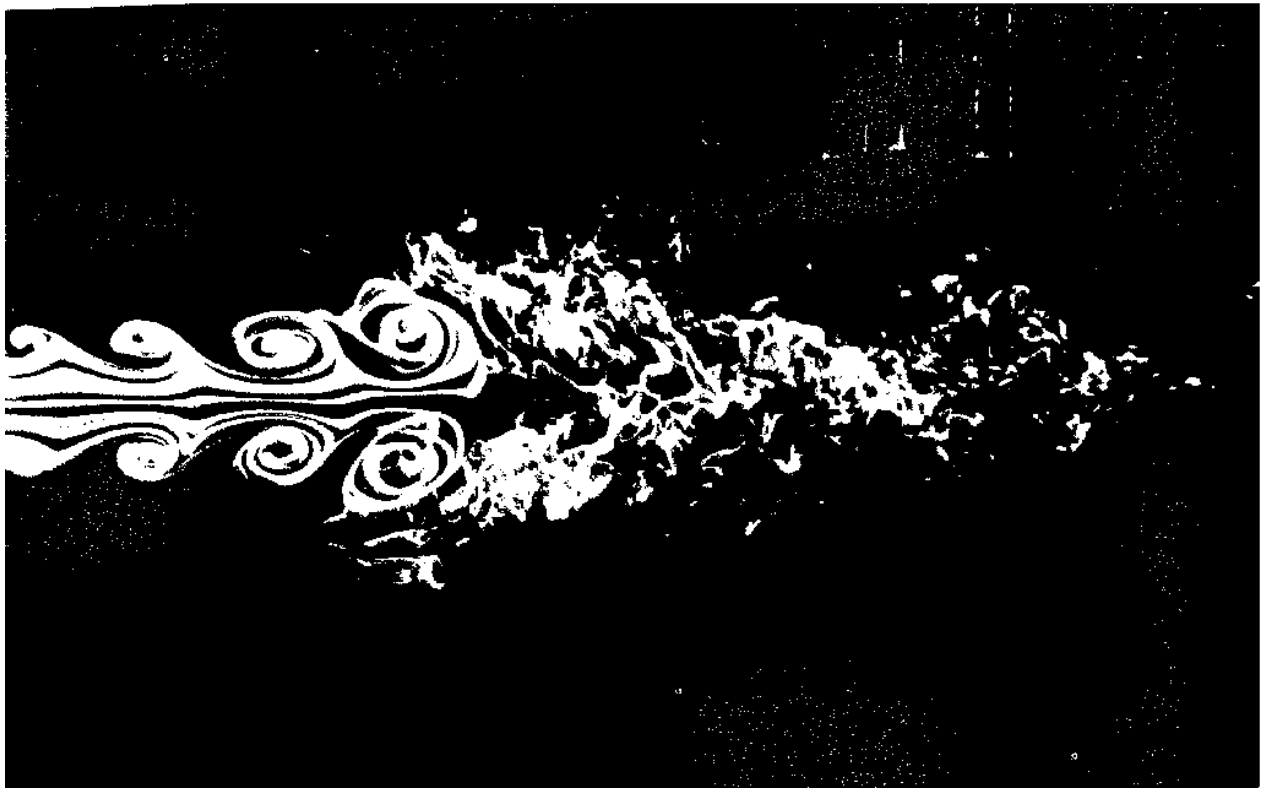

Figure 9: Instability of an axisymmetric jet (Drubka and Nagib).

Vorticity filaments

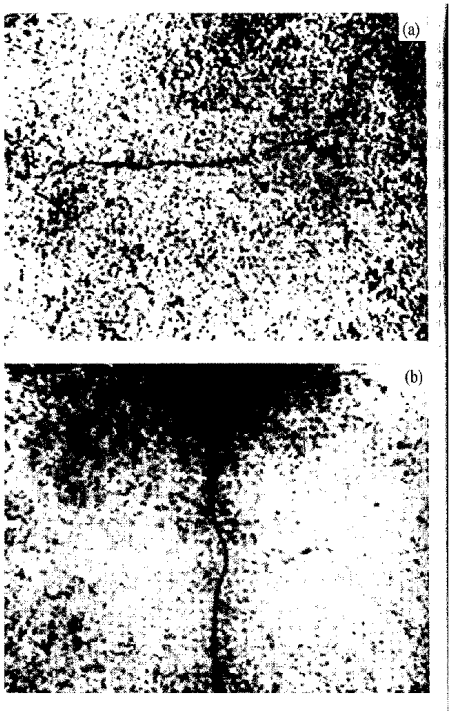

Figure 10: Images of high concentrations of vorticity in water seeded with small bubbles for visualisation.

Vorticity filaments

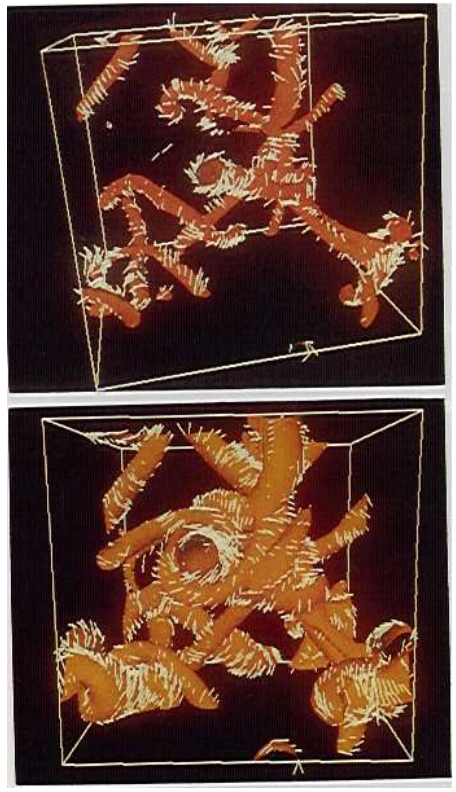

Figure 11: Iso-vorticity surfaces with superimposed velocity vectors (Sain, et al., 1997) from a 64^3 simulation.

Vorticity filaments

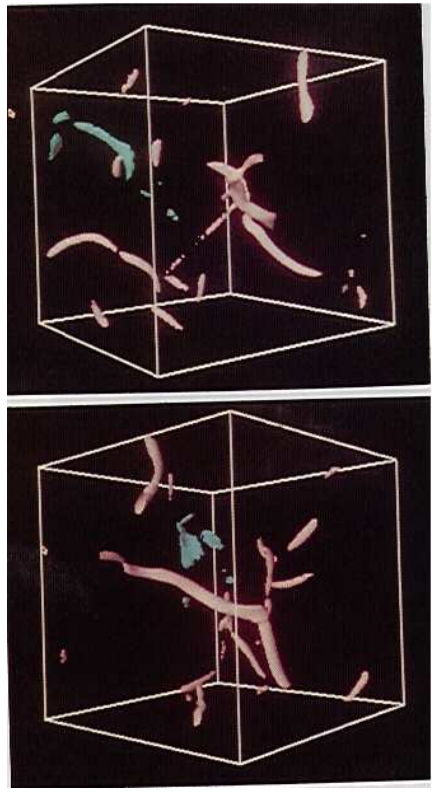

Figure 12: Iso-vorticity (cream) and isodissipation (blue) surfaces (Sain, et al., 1997) from a 64^3 simulation.

Vorticity filaments

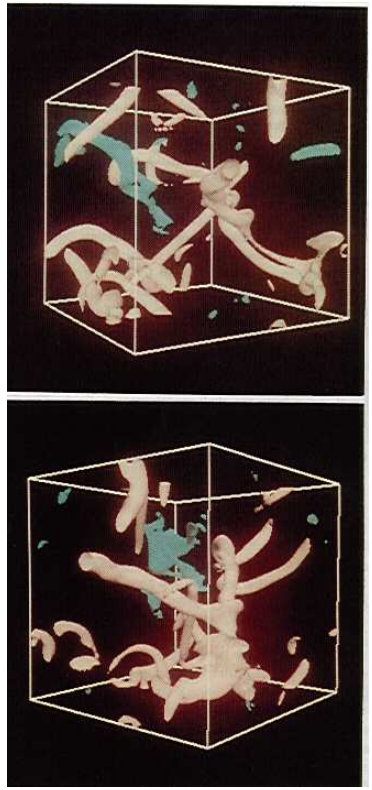

Figure 13: Iso-vorticity (cream) and isodissipation (blue) surfaces (Sain, et al., 1997) with lower ω/ω_{max} and ϵ/ϵ_{max} ratios than in the previous figure

High-performance computing

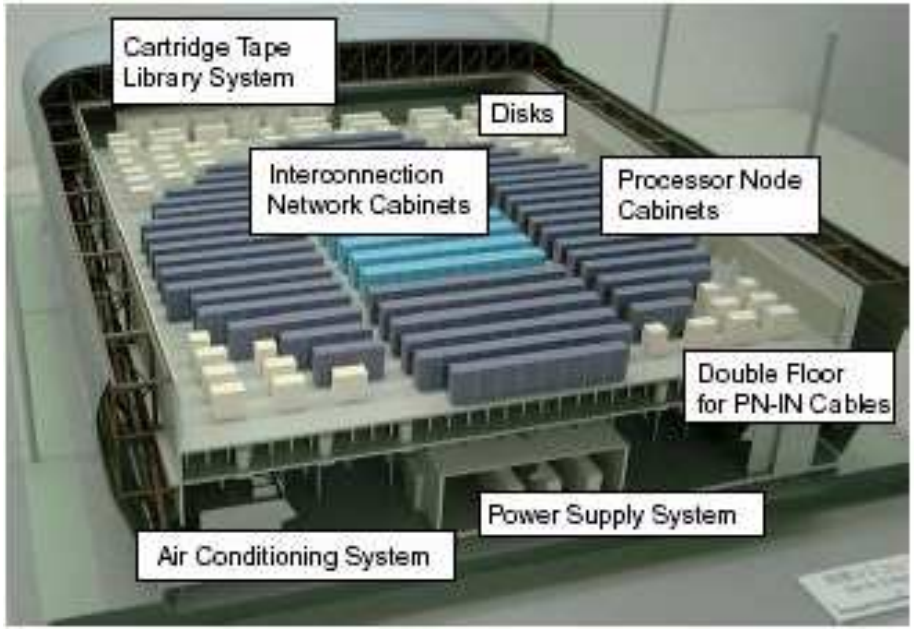

Figure 14: Model of the Earth Simulator, Japan. This computer is in a 50m X 65m X 17 m, two-storeyed building.

Vorticity filaments

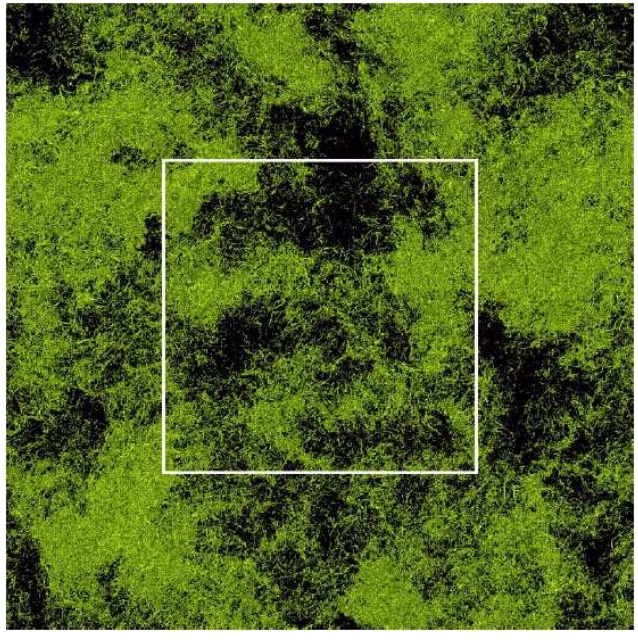

Figure 15: Intense-vorticity isosurfaces from a 4096^3 simulation on the Earth Simulator (Y. Kaneda, et al., 2003).

Vorticity filaments

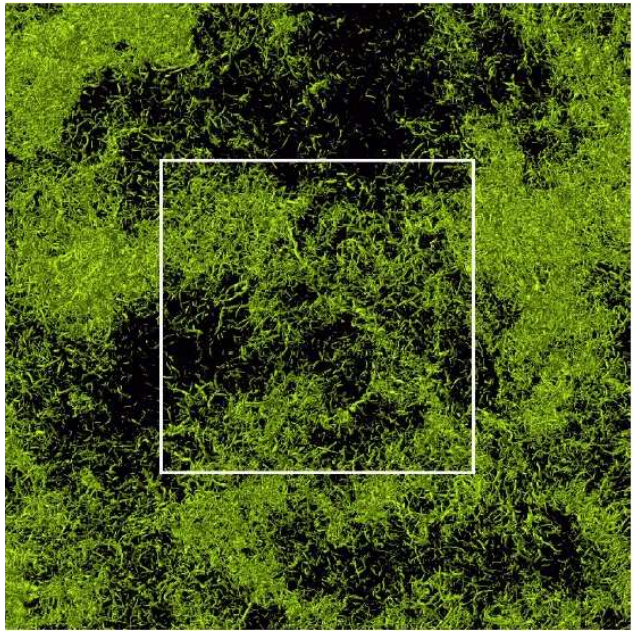

Figure 16: A closer view of the inner square region of the previous figure.

Vorticity filaments

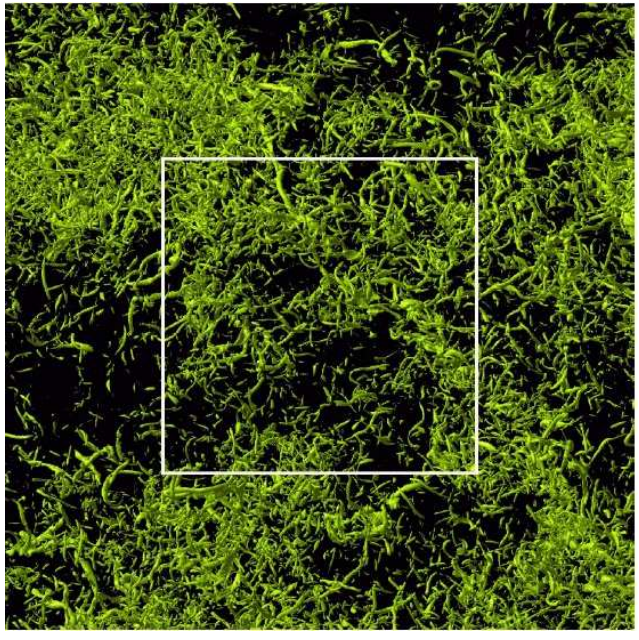

Figure 17: A closer view of the inner square region of the previous figure.

Vorticity filaments

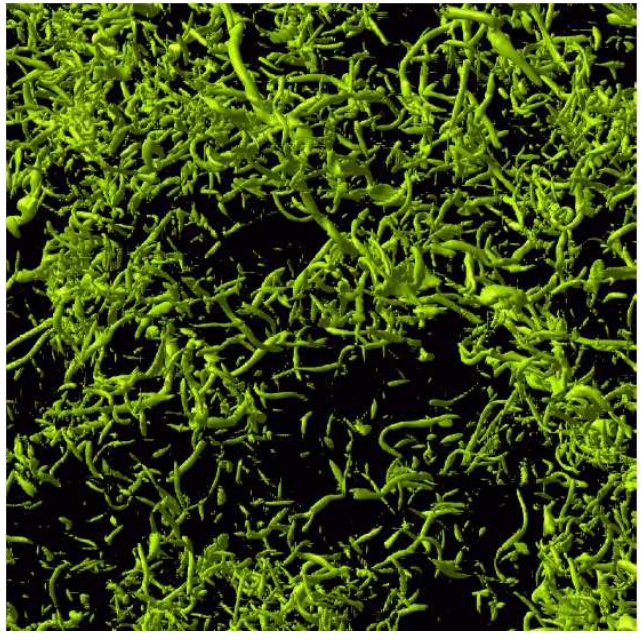

Figure 18: A closer view of the inner square region of the previous figure.

Probabilistic description

- Why do we need a probabilistic description of turbulence (see, e.g., U. Frisch)?
- Velocity signals from turbulent flows are disorganised.
- They are unpredictable in their detailed behaviour.
- Some average properties of the signals are quite reproducible.

Wind tunnel

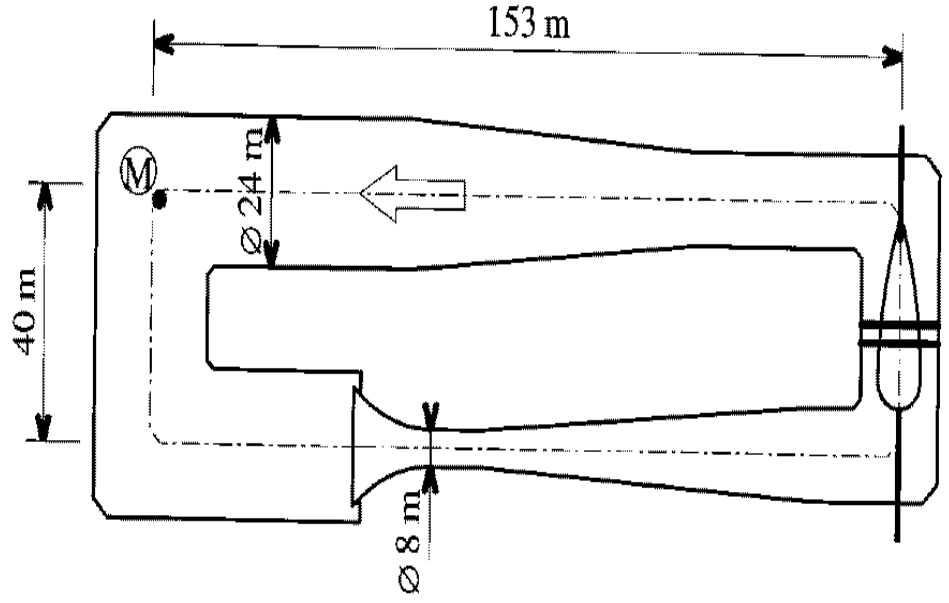

Fig. 5.2. The S1 wind tunnel of ONERA.

Figure 19: A schematic drawing of the S1 wind tunnel at ONERA.

Time series

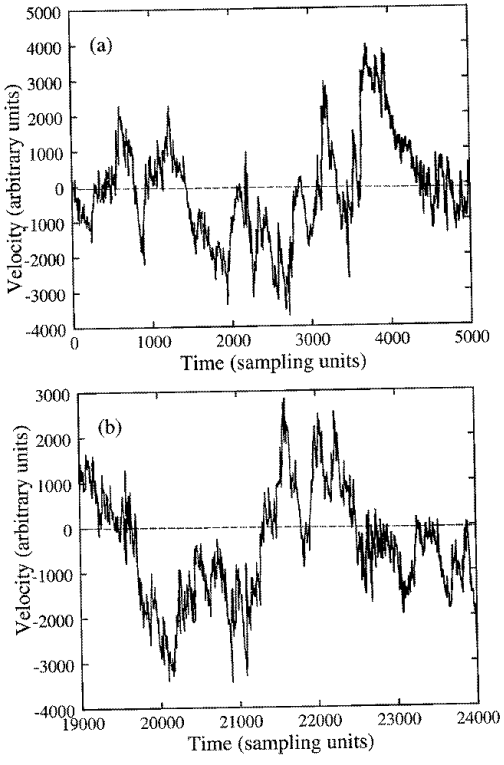

Figure 20: One-second traces of a signal recorded at the S1 wind tunnel of ONERA by Gagne and Hofinger.

Histograms

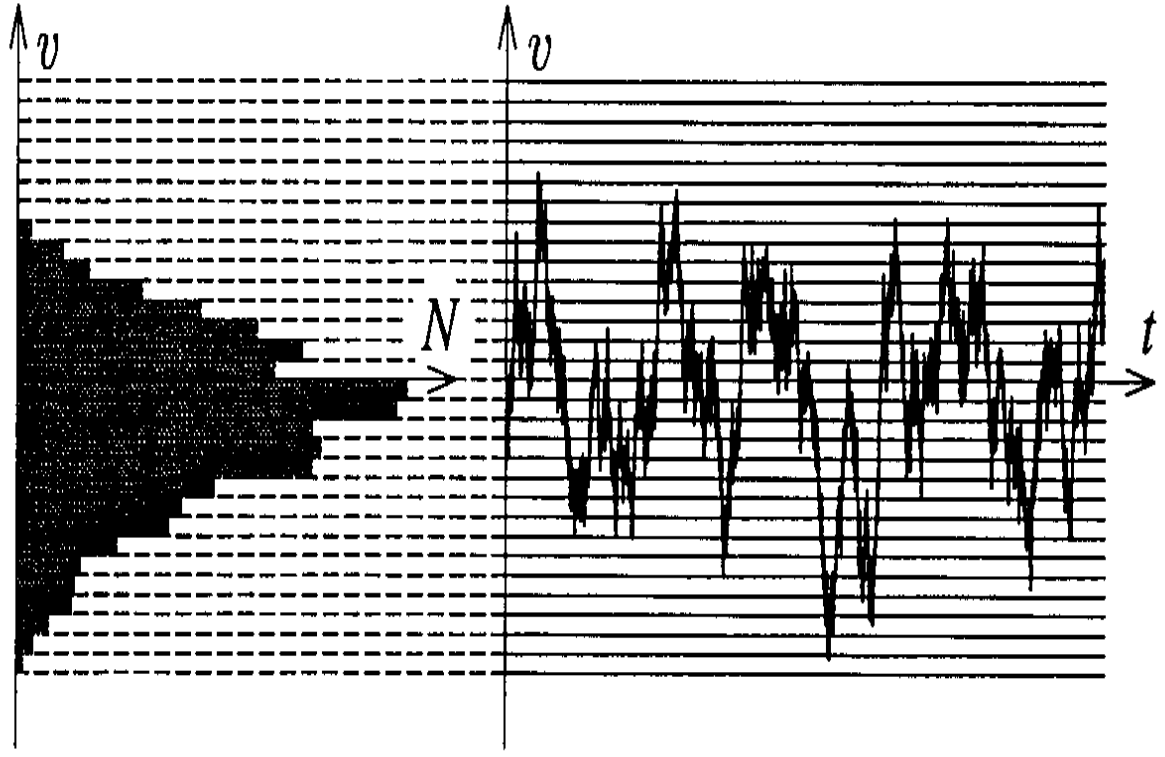

Figure 21: Construction of the histogram of a signal by binning.

Structure functions

Second order, longitudinal structure function:

$$\mathcal{S}_2(l) \equiv \langle \left(\delta v_{||}(l)\right)^2 \rangle; \tag{1}$$

longitudinal velocity increment:

$$\delta v_{||}(\mathbf{r}, \ell) \equiv \left[\mathbf{v}(\mathbf{r}+\ell) - \mathbf{v}(\mathbf{r})\right] . \frac{\ell}{\ell}. \tag{2}$$

Instead of a two-point measurement one often uses the Taylor hypothesis to convert temporal separations to spatial ones.

Taylor hypothesis

If U is the mean flow in the x direction

$$v(t,x) = v'\left(t, x - Ut\right) + U \tag{3}$$

Measure turbulence intensity by

$$I = \frac{\sqrt{\langle v'^2 \rangle}}{U} \ll 1. \tag{4}$$

Relate temporal separations τ to lengths ℓ by

$$\ell = U\tau \tag{5}$$

Reynolds number

$$R_\lambda \equiv \frac{v_{rms}\lambda}{v} \tag{6}$$

Taylor-microscale:

$$\frac{1}{\lambda^2} \equiv \frac{\left\langle (\delta_1 v_1)^2 \right\rangle}{v_{rms}^2}. \tag{7}$$

Reynolds number

Root-mean-square velocity:

$$v_{rms} = (2E/3)^{1/2} \qquad \langle (\partial_1 v_1)^2 \rangle = (2/15)\Omega \tag{8}$$

E: mean energy; Ω : mean enstrophy.

$$\frac{1}{\lambda^2} = \frac{\Omega}{5E'} \tag{9}$$

Structure functions

Order-p, equal-time, longitudinal velocity structure function:

$$\begin{aligned} S_p(l) &\equiv \langle \delta v(l,t)^p \rangle, \\ \delta v(l,t) &\equiv [\vec{v}(\vec{r}+\vec{l},t) - \vec{v}(\vec{r},t)] \cdot (\vec{l}/l), \end{aligned} \tag{10}$$

then for l in the *inertial range* we have

$$S_p(l) \sim l^{\zeta_p}. \tag{11}$$

$\vec{v}(\vec{r})$: Eulerian velocity at the point $\vec{r}$;

Inertial range

inertial range: $eta_d \ll l \ll L$; L : length scale at which energy is pumped into the fluid; η_d: the spatial scale at

which dissipative losses become significant

$\langle\rangle$:average over the nonequilibrium statistical steady state that obtains in the turbulent fluid.

Multiscaling

The power law of Eq. (11) is reminiscent of the behaviour of correlation functions in critical phenomena

But simple scaling must be replaced by multiscaling, i.e.,

ζ_p is a nonlinear, convex function of p

Multiscaling

For example, in the She-Leveque formula

$$\zeta_p^{SL} = (p/9) + 2[1 - (2/3)^{p/3}], \tag{12}$$

which provides a good parametrization of experimental and numerical data for the multiscaling exponents ζ_p.

K41 scaling

Scaling in Fluid Turbulence Kolmogorov 1941 (K41)

Figure 22: A.N. Kolmogorov

K41 scaling

Turbulence is homogeneous and isotropic far away from boundaries and statistically steady.

Energy is pumped in at lengths $\sim L$ and dissipation is significant only for lengths $\lesssim \eta_d$.

In the *inertial range* , $\eta_d \ll l \ll L$, all statistical quantities are independent of both the forcing term and the viscosity.

K41 scaling

Energy cascades (Richardson) down the inertial range till it is dissipated in the dissipation range.

Thus $S_p(l)$ can depend only on l and the rate of energy dissipation per unit volume per unit mass ϵ, which approaches a positive, constant value at large Re in three dimensions (zeroth law of turbulence).

Dimensional analysis now leads to $S_p(l) \sim (\epsilon l)^{p/3}$ whence

$$\zeta_p^{K41} = p/3. \tag{13}$$

K41 scaling

Experiments and direct numerical simulations (DNS) indicate that the K41 scaling result does not hold and multiscaling deviations from it are particularly apparent for $p > 3$.

The energy spectrum $E(k) \sim k^2 |\mathbf{v}(\mathbf{k})|^\mathbf{2}$ scales as $k^{-5/3}$ at the level of K41.

Richardson cascade

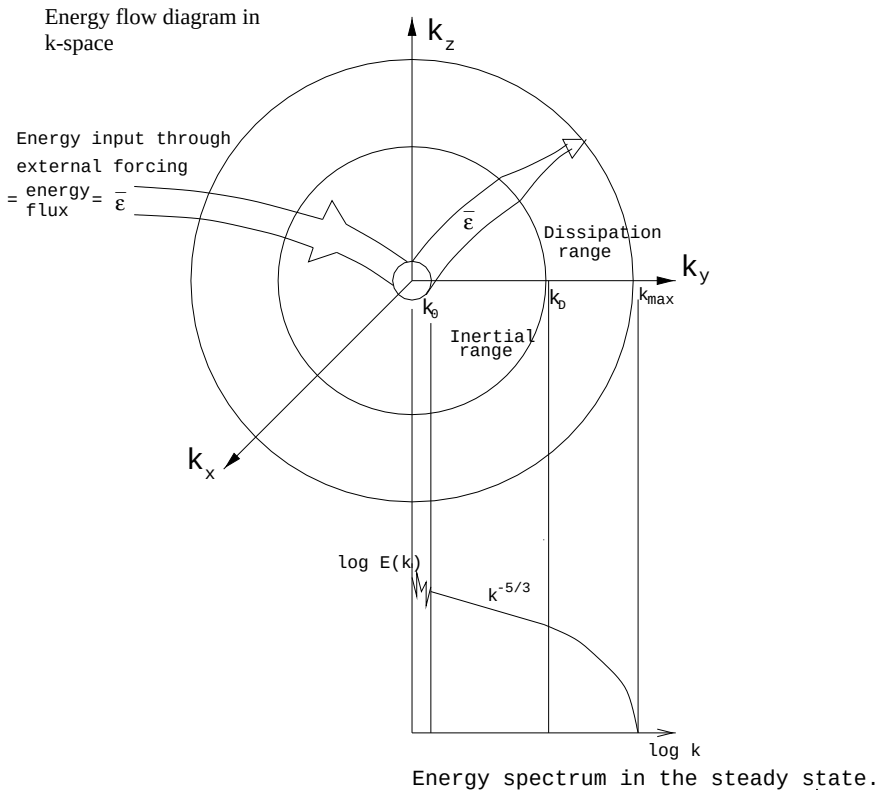

Figure 23: A schematic illustration of the Richardson cascade.

Zeroth law

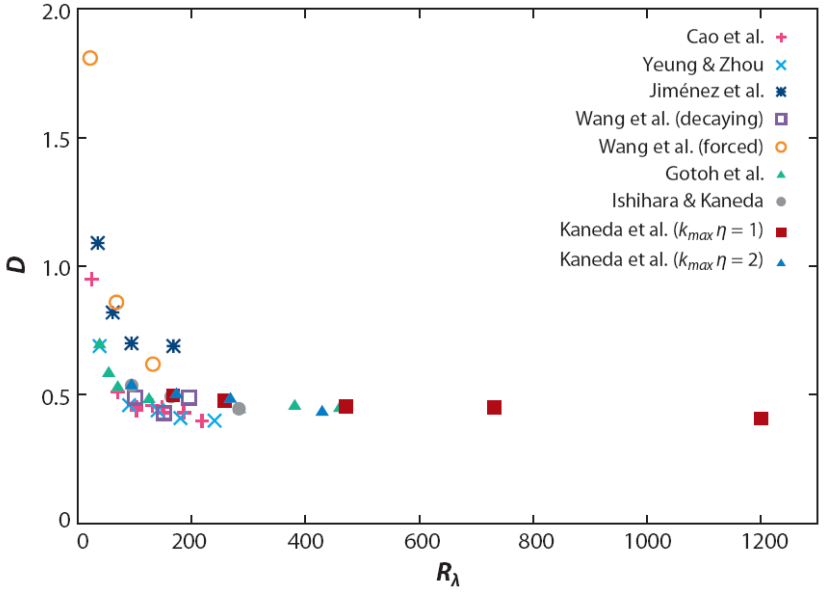

Figure 2

Normalized dissipation rate D versus R_λ. Direct numerical simulation data from Gotoh et al. (2002), Ishihara & Kaneda (2002), and Kaneda et al. (2003), together with those compiled by Sreenivasan (1998), i.e., the data from Cao et al. (1999), Jiménez et al. (1993), Wang et al. (1996), and Yeung & Zhou (1997). Figure redrawn from Kaneda et al. 2003.

Figure 24: Illustration of the zeroth law of turbulence (figure from Kaneda, et al. (2003)).

Zeroth law

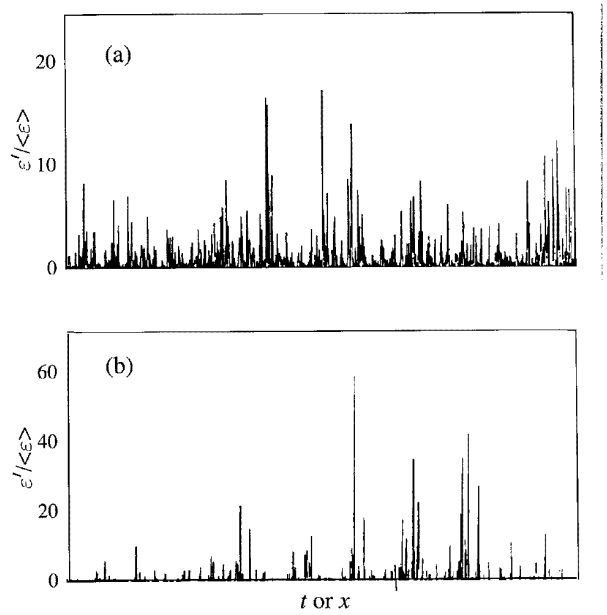

Figure 25: Typical signals of a representative of the local dissipation illustrating the intermittency of energy dissipation. Data are from (a) a laboratory boundary layer and (b) the atmospheric surface layer (Meneveau and Sreenivasan,

PDFs

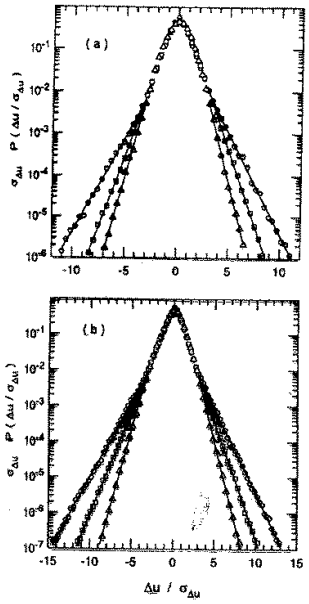

Figure 26: PDFs of velocity differences for r in the inertial range from (a) wind-tunnel and (b) atmospheric surface layers (Praskovsky and Oncley).

Structure functions

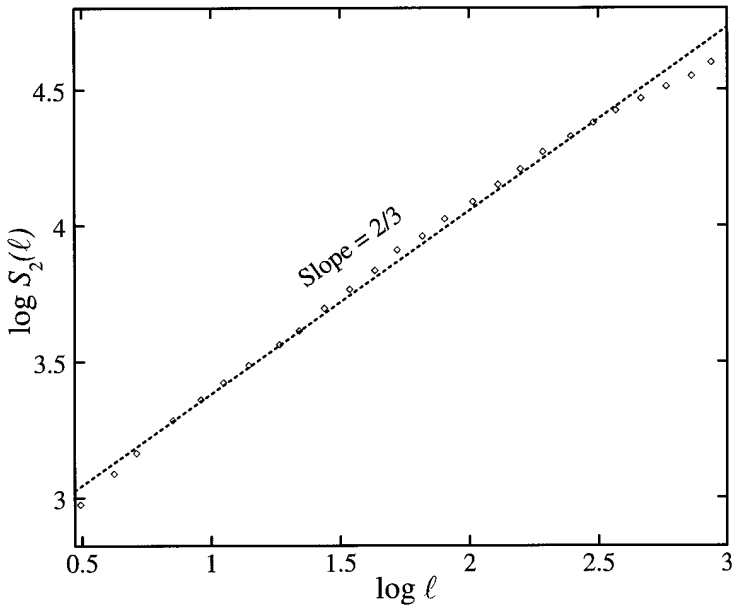

Figure 27: log-log plot of the second=order sructure function in the time domain for data from the S1 wind tunnel of ONERA (Gagne and Hopfinger).

Structure functions

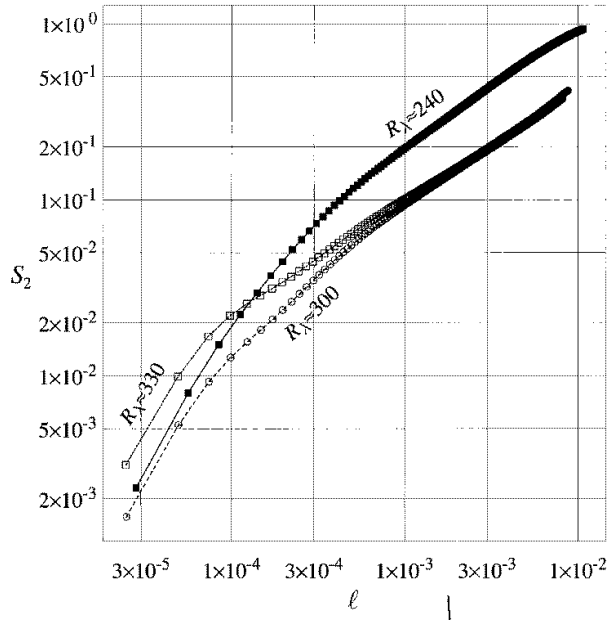

Figure 28: Second-order structure function in the space doamin by the RELIEF technique (Noullez, et al., 1996).

Energy spectrum

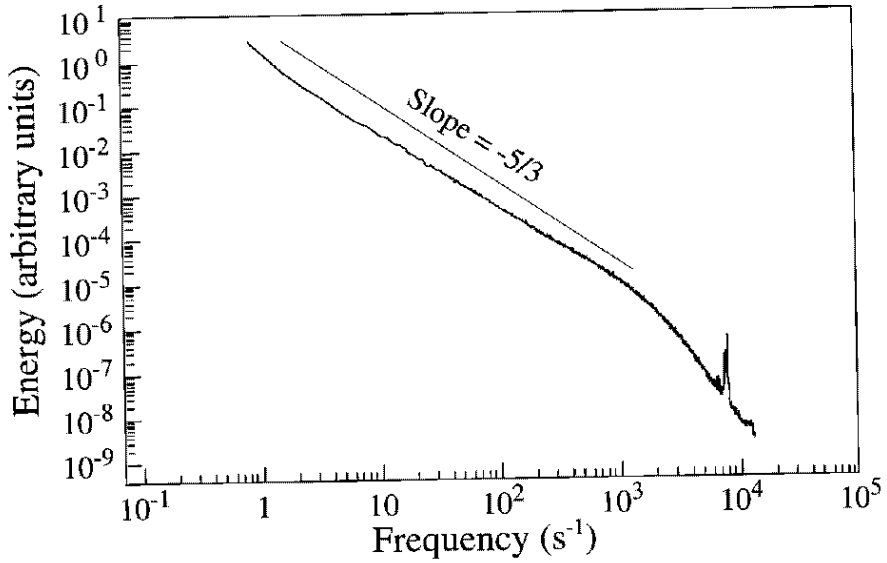

Figure 29: Energy spectrum in the time domain for data from the S1 wind tunnel of ONERA at $Re_\lambda = 2720$ (Gagne and Hopfinger).

Energy spectrum

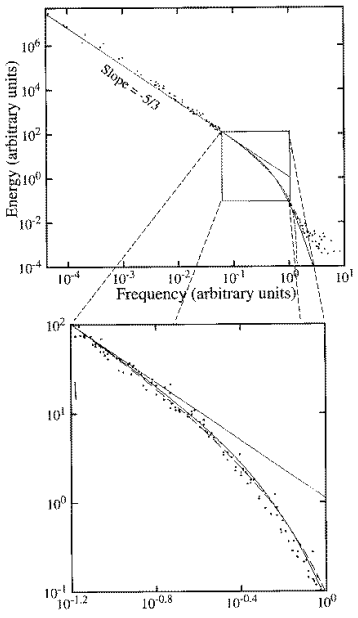

Figure 30: Energy spectrum in the time domain and enlargement showing the beginning of the dissipation range for a tidal channel (Grant, et al., (1962).)

Energy spectra

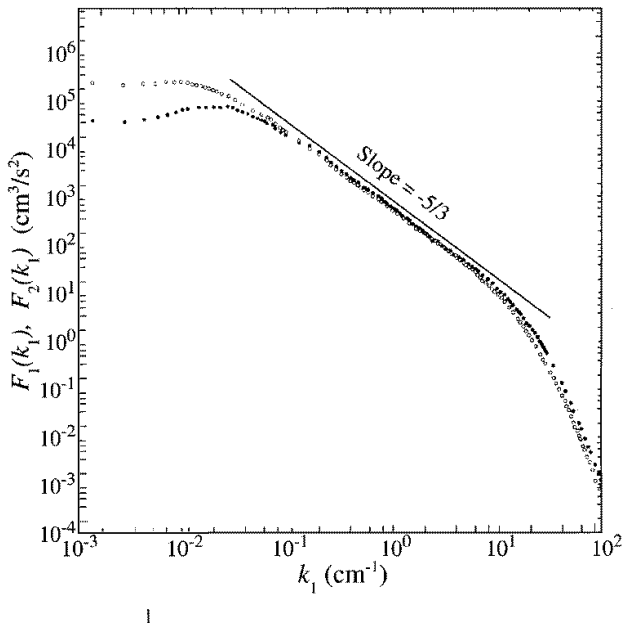

Figure 31: Log-log plot of the energy spectra in the time domain in a jet for streamwise (open circles) and lateral components (black circles) (Champagne 1978).

Energy spectrum

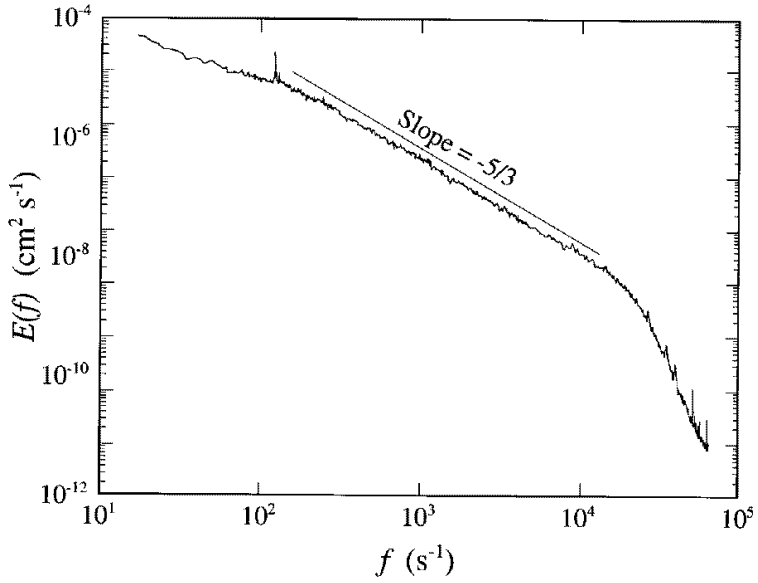

Figure 32: Log-log plot of the energy spectrum (time domain) in a low-temperature helium-gas flow between counter-rotating cylinders ($Re_\lambda = 1200$) (Maurer, et al., 1994).

Energy spectrum

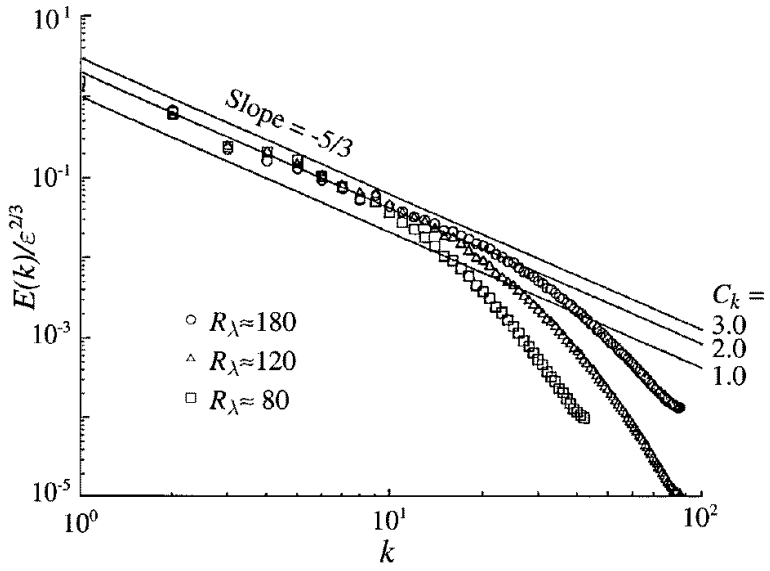

Figure 33: Energy spectra in the space domain from a 256^3 simulation (T. Sanada and K. Ishii).

Statistical steady state

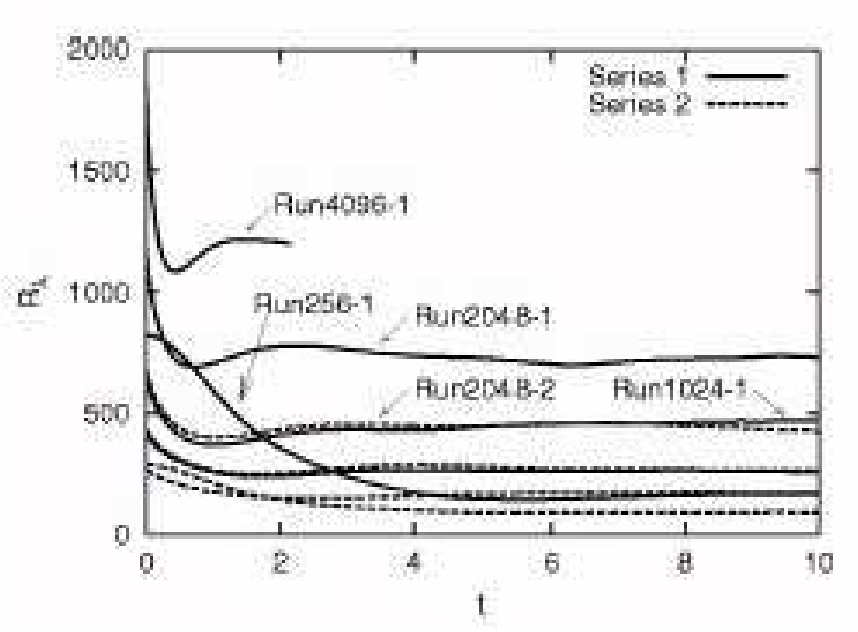

Figure 34: Re_λ versus time t (figure from Kaneda, et al. (2003)).

Statistical steady state

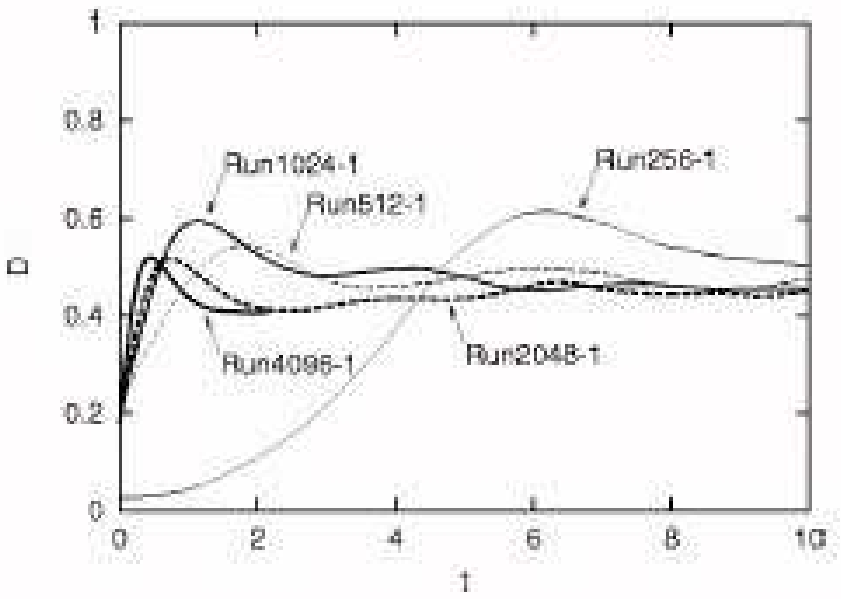

Figure 35: Dimensionless dissipation versus time t (figure from Kaneda, et al. (2003)).

Energy spectrum

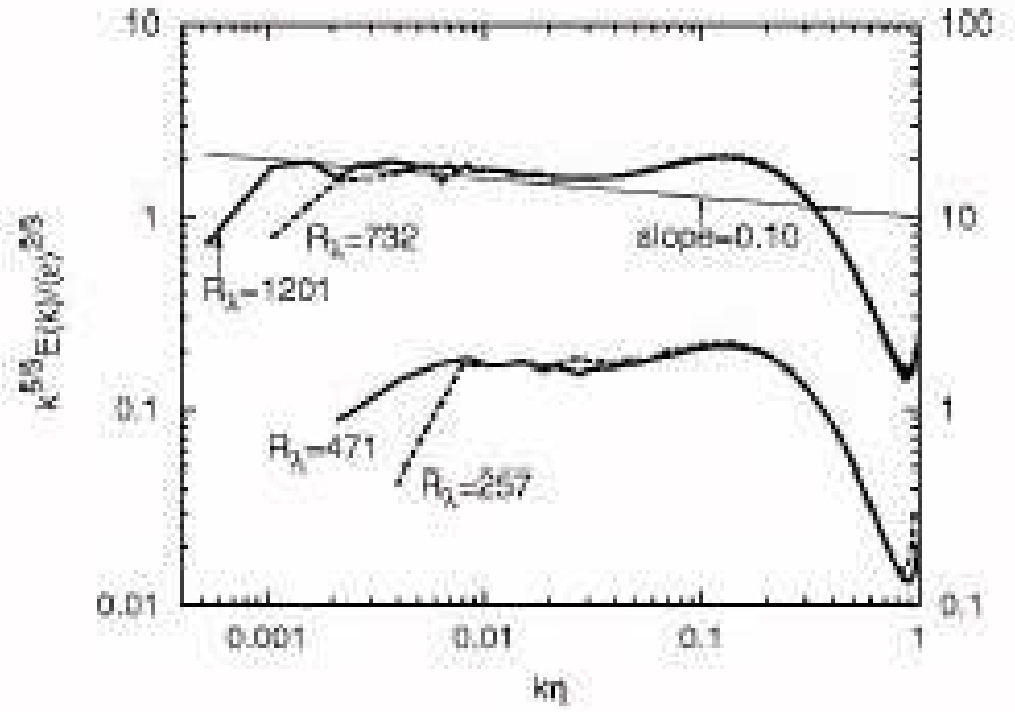

Figure 36: The energy spectrum versus k (figure from Kaneda, et al. (2003)).

Structure functions

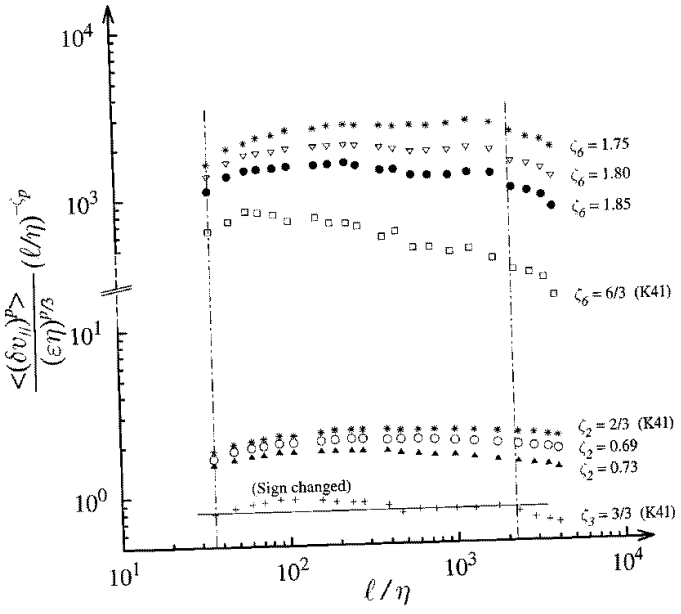

Figure 37: Structure functions of orders 2, 3, and 6 in the time domain, compensated by the guesses for the power-law factors for data from the S1 wind tunnel at ONERA (Gagne, 1987).

Structure functions

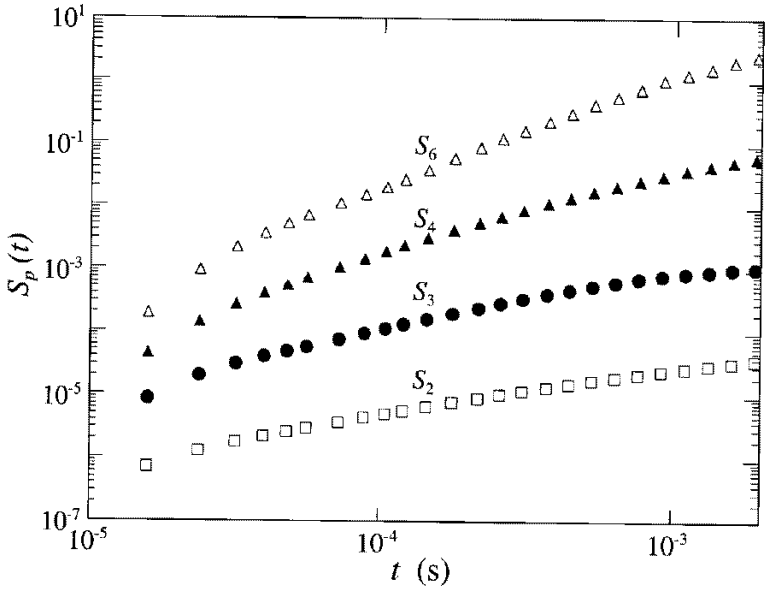

Figure 38: Structure functions of order 2, 3, 4, and 6 in the time domain for a low-temperature helium gas (Maurer, et al., 1994).

Multiscaling

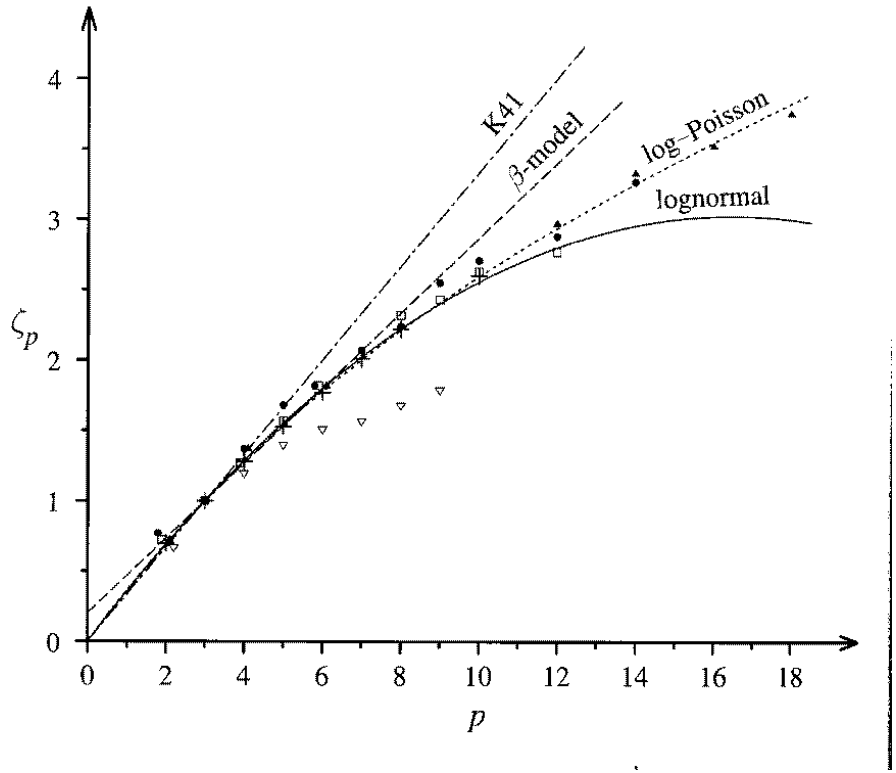

Figure 39: Exponents ζ_p versus order p: data from several experiments (see U. Frisch's book) and curves from different models used to fit such data

Multiscaling

- Partial Differential Equations (PDEs): Euler, Navier-Stokes, MHD, Burgers, Passive-Scalar, and BMHD equations.
- Collections of Ordinary Differential Equations (ODEs): Shell Models for fluid and MHD turbulence (e.g., GOY, SABRA, and their MHD analogues).

Euler Equation

Newton's second law of motion yields the Euler equation:

$$\frac{\partial \mathbf{u}}{\partial t} + \mathbf{u}.\nabla \mathbf{u} = -\frac{1}{\rho}\nabla p + \mathbf{f}/\rho, \tag{14}$$

$\mathbf{u}$:fluid velocity; p:pressure; ρ:fluid mass density; $\mathbf{f}$:external force.

Euler

Figure 40: Leonhard Euler (1707-1783)

Incompressibility

Continuity Equation $\frac{\partial \rho}{\partial t} + \nabla \cdot (\rho \mathbf{u}) = 0$

For an incompressible fluid this is replaced by the condition $\nabla \cdot \mathbf{u} = 0$.

Navier and Stokes

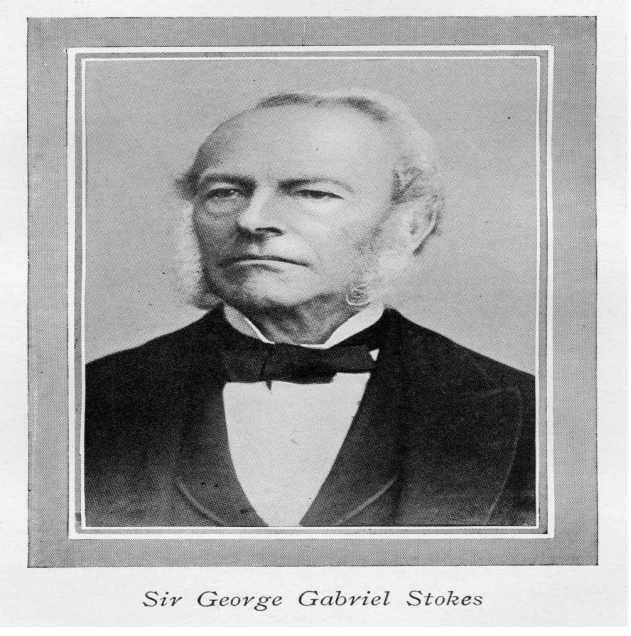

Sir George Gabriel Stokes

Claude-Louis Navier (1785-1836) and George Gabriel Stokes (1819-1903).

Navier-Stokes Equation

$$\rho \left[\frac{\partial \mathbf{u}}{\partial t} + (u \cdot \nabla)u\right] = -\nabla p$$

$$+ \quad \eta \nabla^2 \mathbf{u} + (\zeta + \frac{1}{3}\eta)\nabla(\nabla \cdot \mathbf{u}) + \mathbf{f}.$$

ν: **shear viscosity;** ζ: **bulk viscosity.**

Navier-Stokes Equation

For an incompressible fluid

$$\nabla \cdot \mathbf{u} = 0, \tag{15}$$

so the bulk-viscosity part does not appear in the NS equation; the pressure is determined by

$$\nabla^2 p = -\rho \nabla \cdot (\mathbf{u}.\nabla \mathbf{u}). \tag{16}$$

This is valid at low Mach numbers, i.e., if typical velocities are much less than the speed of sound in the fluid.

Incompressibility

Incompressibility leads to:

$$\begin{aligned} \partial_t \mathbf{u} &+ (\mathbf{u}\cdot\nabla)\mathbf{u} = \\ \nu &\nabla^2\mathbf{u} - \nabla p/\rho + \mathbf{f}/\rho, \end{aligned}$$

with
$\nabla \cdot \mathbf{u} = 0;$
$\nu = \eta/\rho$
the kinematic viscosity.

Shell Models

Simple ODE models for fluid or other (e.g., MHD) turbulence.
Essential ingredients of such shell models:

- Concentrate on the one-dimensional cascade of energy from low to high wavevectors.
- Label Fourier components of the velocities by a discrete set of logarithmically spaced wave vectors $k_n = k_0 \lambda^n$.

Shell Models

- The dynamical variables are the complex, scalar velocities v_n for each shell n.
- The velocity in a given shell is affected directly only by those in nearest- and next-nearest-neighbour shells.
- The system is forced at small wave vectors.
- Dissipation occurs principally at large wave vectors.
- Thus energy cascades from small to large wave vectors.

Shell Models

Advantages:

- Since they are much simpler than the Navier-Stokes equation, they can be studied in much greater detail; very large values of Re_λ and hence larger inertial ranges can be obtained.
- They yield multiscaling and multiscaling exponents akin to those seen in experiments.

Shell Models

- A shell model can be viewed as a greatly simplified, quasi-Lagrangian version of the Navier-Stokes equation since they do not have a direct sweeping effect (see below).

Shell Models

Disadvantages:

- Since the wave vectors and velocities are scalars, strictly speaking they have no vorticity or coherent structures.
- Since the velocity in a given shell is affected directly only by those in nearest- and next-nearest-neighbour shells, they do not have the analogue of the sweeping effect present in the Navier-Stokes equation.

Shell Models

- That is large eddies (i.e., v_n with small n) cannot drive, directly, small eddies (i.e., v_n with large n).
- Even though these models are much simpler than the Navier-Stokes equation, they have to be studied numerically.

GOY Shell Model

$\frac{d}{dt}v_n = iC_n - \nu k_n^2 v_n + f_n$, **with**

$$\begin{aligned} C_n &= \left(ak_n v_{n+1} v_{n+2}\right. \\ &+ \left. bk_{n-1} v_{n-1} v_{n+1} + ck_{n-2} v_{n-1} v_{n-2}\right)^*; \end{aligned}$$

GOY Shell Model

$a, b,$ and c can be fixed upto a constant by demanding that these equations satisfy all the conservation laws (analogues of energy and helicity) in the unforced, inviscid limit.

Burgers Equation

Simplest form: A one-dimensional model (not incompressible) with no pressure term.

- Galilean invariant.
- Preserves the analogue of the kinetic energy in the unforced, inviscid limit.

Burgers Equation

- Applications in cosmology, condensed-matter physics; can be used as a testing ground for ideas about turbulence.
- Can be linearised by the Hopf-Cole transformation but can still show interesting bifractal scaling.

Burgers Equation

$$\frac{\partial v}{\partial t} + \frac{1}{2}\frac{\partial}{\partial x}v^2 = \nu\frac{\partial^2 v}{\partial x^2} + f.$$

Polymeric Turbulence

Navier-Stokes and FENE-P equations

Polymeric Turbulence

- Navier-Stokes(NS) with Polymer Additives:

  3D, unforced, incompressible, NS with dilute polymer solution

$$\frac{\partial \mathbf{u}}{\partial t} + (\mathbf{u}\cdot\nabla)\mathbf{u} \;=\; -\nabla p + \nu\nabla^2\mathbf{u} + \nabla\cdot\mathcal{T},$$

  where

  - $\mathbf{u}(\mathbf{x},t)$: fluid velocity; point $\mathbf{x}$; time t;
  - ν: Kinematic viscosity of the fluid;
  - $\mathcal{T}$: polymer contribution to the fluid stress;

  $\nabla\cdot\mathbf{u} = 0$ enforces incompressibility.

FENE-P Shell Model

- Kalelkar *et.al.*(2005), Benzi *et.al.*(2003):

$$\frac{du_n}{dt} = \Phi_{n,uu} - \nu_s k_n^2 u_n + \frac{\nu_p}{\tau_p(1-\sum_n |b_n|^2)}\Phi_{n,bb},$$

$$\frac{db_n}{dt} = \Phi_{n,ub} - \Phi_{n,bu} - \frac{1}{\tau_p(1-\sum_n |b_n|^2)} b_n$$

  where u_n and b_n are complex, scalar variables representing the velocity and the (normalized) polymer end-to-end vector fields, $k_n = k_0 2^n$ are the discrete wavenumbers for the shell index N

- Polymer concentration $c \equiv \nu_p/\nu_s$

Polymeric Turbulence

$$\Phi_{n,vv} = i(a_1 k_n v_{n+1} v_{n+2} + a_2 k_{n-1} v_{n+1} v_{n-1} + a_3 k_{n-2} v_{n-1} v_{n-2})]$$

$$\Phi_{n,bb} = -i(a_1 k_n b_{n+1} b_{n+2} + a_2 k_{n-1} b_{n+1} b_{n-1} + a_3 k_{n-2} b_{n-1} b_{n-2})$$

$$\Phi_{n,vb} = i(a_4 k_n v_{n+1} b_{n+2} + a_5 k_{n-1} v_{n-1} b_{n+1} + a_6 k_{n-2} v_{n-1} b_{n-2})$$

$$\Phi_{n,bv} = -i(a_4 k_n b_{n+1} v_{n+2} + a_5 k_{n-1} b_{n-1} v_{n+1} + a_6 k_{n-2} b_{n-1} v_{n-2})$$

Magnetohydrodynamics

Navier-Stokes equation and the Lorentz force.

Faraday's law and Ohm's law.

Often use incompressibility though for many physical situations this may not hold, e.g., in the solar wind and on the sun's surface.

Magnetohydrodynamics

$$
\begin{aligned}
\partial_t \vec{v} &+ (\vec{v}\cdot\nabla)\vec{v} = \nu_v \nabla^2 \vec{v} \\
-\nabla(p &+ b^2/2)/\rho + (\vec{b}\cdot\nabla)\vec{b} + \vec{f_v}/\rho, \\
\partial_t \vec{b} &= \nabla\times(\vec{v}\times\vec{b}) \\
&+ \nu_b \nabla^2 \vec{b} + \vec{f_b},
\end{aligned}
$$

Magnetohydrodynamics

with $\vec{b}$ the magnetic field, ν_v and ν_b the fluid and magnetic kinematic viscosities and $\vec{f_v}$ and $\vec{f_b}$ the forcing terms in the velocity and magnetic-field equations.
Furthermore

$$\begin{aligned} \nabla \cdot \vec{v} &= 0; \\ \nabla \cdot \vec{b} &= 0. \end{aligned}$$

Magnetohydrodynamics

- It is often convenient to use the Elsässer variables $\vec{z}^{\pm} \equiv \vec{v} \pm \vec{b}$.
- If we have a mean magnetic field $\vec{B}_0$, then, in the MHD equations, $\vec{b} \rightarrow \vec{B}_0 + \vec{b}(\mathbf{r}, \mathbf{t})$.
- If $\vec{B}_0 \neq 0$ we get Alfven waves with a frequency that depends linearly on $|\vec{B}_0|$.

Magnetohydrodynamics

Our Shell Model for 3DMHD Turbulence

$$\begin{aligned} \frac{dz_n^{\pm}}{dt} &= ic_n^{\pm} - \nu_+ k_n^2 z_n^{\pm} \\ &- \nu_- k_n^2 z_n^{\pm} + f_n^{\pm}, \end{aligned}$$

with $z_n^{\pm} \equiv (v_n \pm b_n)$ **complex, scalar Elsässer variables and**

Magnetohydrodynamics

$$
\begin{aligned}
c_n^{\pm} &= [a_1 k_n z_{n+1}^{\mp} z_{n+2}^{\pm} \\
&+ a_2 k_n z_{n+1}^{\pm} z_{n+2}^{\mp} \\
&+ a_3 k_{n-1} z_{n-1}^{\mp} z_{n+1}^{\pm} \\
&+ a_4 k_{n-1} z_{n-1}^{\pm} z_{n+1}^{\mp} \\
&+ a_5 k_{n-2} z_{n-1}^{\mp} z_{n-2}^{\pm} \\
&+ a_6 k_{n-2} z_{n-1}^{\mp} z_{n-2}^{\pm}]^{*}.
\end{aligned}
$$

Burgers Model Analogue of MHD

$$\frac{\partial v}{\partial t} + B_o \frac{\partial b}{\partial x} + \frac{1}{2}\frac{\partial}{\partial x} v^2 + \frac{1}{2}\frac{\partial}{\partial x} b^2 = \nu \frac{\partial^2}{\partial x^2} v + f_1; \tag{17}$$

Magnetohydrodynamics

$$\frac{\partial b}{\partial t} + B_o \frac{\partial v}{\partial x} + \frac{\partial}{\partial x}(vb) = \mu \frac{\partial^2}{\partial x^2} b + f_2.$$

Passive Scalars

The Passive-Scalar Equation

$$\begin{aligned} \frac{\partial \theta}{\partial t} &+ \vec{v} \cdot \nabla \theta \\ &= \kappa \nabla^2 \theta + f(\mathbf{r}, \mathbf{t}), \end{aligned}$$

Passive Scalars

with $\theta(\mathbf{r},\mathbf{t})$ the passive scalar field, $\vec{v}(\mathbf{r},\mathbf{t})$ the turbulent velocity field that drives the passive scalar, and $f(\mathbf{r},\mathbf{t})$ the external force.

In some cases a stochastic velocity field is used as an input (Gawedzki, et al., RMP (2001)).

Calculations

Types of Calculations

- Rigorous results on existence, etc., of solutions.
- Linear (or more sophisticated) stability analysis about simple flows.
- Renormalized perturbation theory for stochastically forced models.

Calculations

- Closures, e.g., the direct interaction approximation (DIA).
- Numerical studies, either direct numerical simulation (DNS) or various levels of turbulence modelling, e.g., $k - \epsilon$ and large-eddy smulations (LES).
- We will concentrate on DNS here.

Boundary Conditions

- The normal component of the velocity must vanish at the boundary (both for the Euler and the Navier-Stokes equations).
- For the Navier-Stokes equation the tangential component of the velocity is also controlled; for rigid boundaries we typically use the no slip condition in which the fluid, at the boundary, has a tangential velocity equal to that of the boundary.

Boundary Conditions

- The pressure also has to satisfy the boundary condition $\hat{n} \cdot \nabla p|_{\partial\Omega} = \rho[\nu \hat{n} \cdot \nabla^2 \vec{u}]|_{\partial\Omega}$.
- For studies of homogeneous, isotropic turbulence it is advantageous to use periodic boundary conditions for the pressure and all components of the velocity (and magnetic field).

Further Background

- Refs.: U. Frisch, Turbulence (Cambridge, 1996); S.B. Pope, Turbulent Flows (Cambridge, 2000); C.R. Doering and J.D. Gibbon, Applied Analysis of the Navier-Stokes Equations (Cambridge, 1995).
- Symmetries, e.g., for the Navier-Stokes equation under space and/or time translations, Galilean transformations (for infinite systems or with periodic boundary conditions), parity, rotations, and scaling.

Further Background

- Conservation laws in the unforced, inviscid limits (e.g., for the Navier-Stokes equation, conservation of momentum, energy, and helicity).
- The generalization of the above conservation laws to balance equations in the presence of forcing and dissipation.
- Eulerian and Lagrangian descriptions.

Further Background

Dimensionless Control Parameters

- Navier-Stokes: Reynolds number (if v_{rms} is held fixed) or the Grashof number (if the force is held fixed).
- MHD: Fluid and magnetic Reynolds numbers and the magnetic Prandtl number (the ratio of fluid and magnetic viscosities).

Further Background

Mathematical Issues

- Existence and smoothness of the solutions of the Navier-Stokes and Euler equations. Similar questions arise for all the equations mentioned above.
- Roughly speaking, the question is whether the solutions develop singularities, in finite time, for arbitrary (or analytic) initial data.
- For a precise statement see the web site of the Clay Mathematics Institute.

Further Background

Physicists' Perspective

- Even if there is some problem with the existence and smoothness of the solutions of the Navier-Stokes, we will not have to worry too much about it since higher-order derivatives (neglected at the Navier-Stokes level) will control it.